1998

Hydrodynamics and equilibrium sediment dynamics of shallow, funnel-shaped tidal estuaries

Carl T. Friedrichs
Virginia Institute of Marine Science, carl.friedrichs@vims.edu

Bruce A. Armbrust

H. E. deSwart

Physics of Estuaries and Coastal Seas, Dronkers & Scheffers (eds) © 1998 Balkema, Rotterdam, ISBN 90 5410 965 3

Hydrodynamics and equilibrium sediment dynamics of shallow, funnel-shaped tidal estuaries

C.T. Friedrichs & B.D. Armbrust
Virginia Institute of Marine Science, College of William and Mary, Va., USA
H.E. de Swart
Institute for Marine and Atmospheric Research, Utrecht University, Netherlands

ABSTRACT: Observations of tidal and sediment properties available for the River Tamar are used to guide perturbation solutions for hydrodynamics and equilibrium sediment dynamics. For net sediment transport, important contributions to velocity at $O(\varepsilon)$ are flood dominance due to internally generated nonlinearity and ebb dominance due to river flow. The advection-dispersion equation is used to solve for tidal variations in depth-integrated suspended sediment concentration. The lowest order balance is between erosion and deposition; the importance of advection is scaled by the ratio of the sediment response time-scale to the tidal time-scale. Analytical solutions show that tidally averaged sediment transport at $O(\varepsilon)$ is due to three dominant effects: (i) flood-dominant tidal asymmetry, (ii) seaward river flow, and (iii) settling/scour lag made effective by along-channel width convergence. The third effect represents a new mechanism for the maintenance of the turbidity maximum. Unlike previous solutions applied to short tidal estuaries of constant width, variation in tidally averaged channel depth is not found to be an important control. Assuming uniform bed erodability, the predicted change in direction of tidally averaged sediment transport coincides with the observed location of the turbidity maximum in the River Tamar. However, an equilibrium sediment budget requires erodability to vary along-channel. An analytical solution is presented for along-channel variation in bed erodability which produces zero net transport of sediment at $O(\varepsilon)$. By assuming a migrating, finite size pool of easily erodable bed sediment, analytical solutions successfully reproduce the along-channel extent and intensity of the high turbidity region along the River Tamar, as well as its response to variations in fresh water discharge.

INTRODUCTION

By studying simplified geometries, insight from diagnostic, analytically based models can be used to constrain dominant sediment transport pathways and equilibrium balances in more complex settings. Highly frictional, strongly funnel-shaped tidal estuaries result in relatively simple analytical solutions for tidal elevation and velocity, including nonlinearities (Friedrichs & Aubrey 1994, hereafter F&A94). Nearly funnel-shaped embayments are common along transgressive tidal coastlines, and observations of tidal velocity, suspended sediment concentration and sediment transport rates from field examples are available in the literature (e.g., Uncles et al. 1985; Uncles & Stephens 1989). In the present paper, analytical solutions for nonlinear tidal velocity are combined with the one-dimensional advection-dispersion equation for sediment concentration to predict the equilibrium sediment balance for strongly frictional funnel-shaped embayments. This approach is an extension of Schuttelaars and de Swart (1996), hereafter S&S96, who applied these equations to short channels of constant width.

The analytical results presented here are in general agreement with previous numerical and observational studies of sediment transport and turbidity maximum development in funnel-shaped macrotidal estuaries. For example, both Allen at al. (1980) and Uncles and Stephens (1989) used one-dimensional numerical models which neglected density induced gravitational circulation to demonstrate that the observed turbidity maximum in the Gironde estuary in France and the Tamar estuary in the U.K. could each be reasonably reproduced by the action of tidal currents and freshwater discharge. They each concluded that in the lower reaches of the estuary, sediment is transported landward by flood

dominance generated by nonlinear tidal hydrodynamics, while landward of the turbidity maximum, sediment is transported seaward by river flow. Uncles and Stephens (1989) also documented a seaward migration of the turbidity maximum with increased river discharge in a manner consistent with the findings of this study. More recently, Uncles et al. (1996) described the seaward movement of unconsolidated bed source material in concert with migration of the turbidity maximum.

The analytical solutions in this paper compliment previous numerical and observational results by (i) providing important insight into the physical parameter combinations which govern the previously inferred processes and (ii) identifying entirely new transport mechanisms and controls. In this paper we use high quality observations of hydrodynamics and sediment dynamics available for the River Tamar (Figure 1; George 1975; Uncles et al. 1985, 1996; Uncles & Stephens 1989) to guide properly scaled analytical solutions for hydrodynamics and equilibrium sediment dynamics in shallow, funnel-shaped tidal estuaries.

1. HYDRODYNAMICS

1.1 Lowest order solution

The geometry we consider is an infinite funnel-shaped channel with exponentially decreasing width,

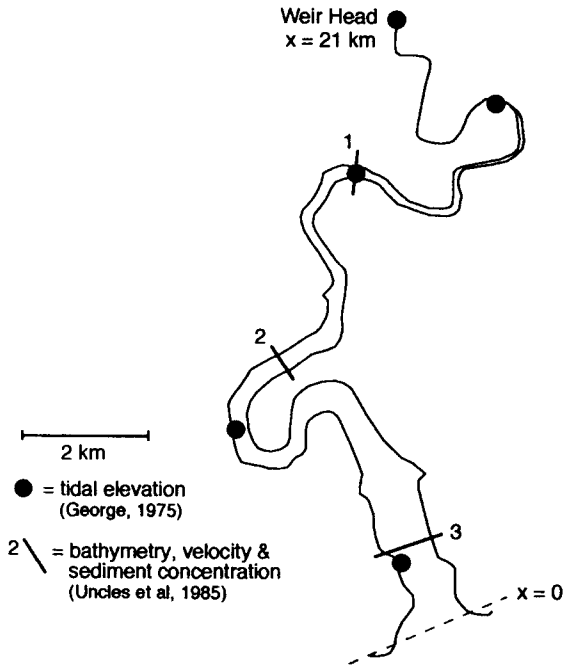

Figure 1. Location of tidal observations along the River Tamar estuary.

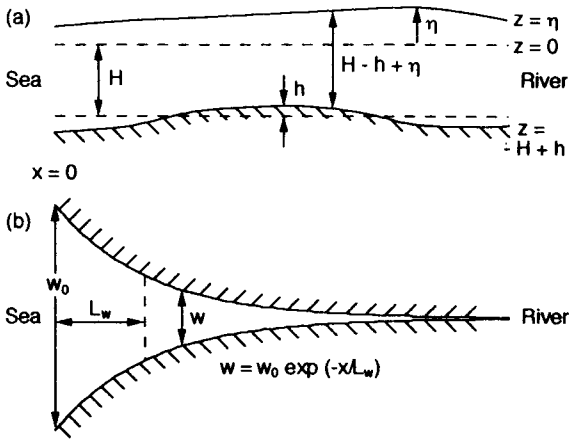

Figure 2. Geometry of idealized tidal estuary: (a) side view; (b) plan view.

$w = w_0\exp(-x/L_w)$, and a rectangular cross section of depth H-h relative to mean ocean level, where H is mean depth of the entire channel and h is the local deviation of the bottom away from depth H (Figure 2).

The relevant one dimensional equations for the hydrodynamics are conservation of mass and momentum:

$$\frac{\partial u}{\partial t} + u\frac{\partial u}{\partial x} = -g\frac{\partial \eta}{\partial x} - c_d\frac{|u|u}{H-h+\eta} \qquad (1)$$

$$w\frac{\partial \eta}{\partial t} + \frac{\partial}{\partial x}\left[uw(H-h+\eta)\right] = 0 \qquad (2)$$

In (1)-(2), u is tidal velocity, t is time, x is distance landward from the ocean, g is acceleration of gravity, η is surface displacement, and c_d is the bottom drag coefficient. The boundary condition at $x = 0$ is a tidal surface displacement of $\eta = A\cos(st) + A_2\cos(2st-\theta_2)$, where s is the dominant tidal frequency, A_2 and θ_2 are the amplitude and phase of the overtide at $x = 0$, and there is a spatially invariant river discharge, Q.

F&A94 present observations and theory indicating the lowest order solution for funnel-shaped estuaries such as the River Tamar is simply

$$\eta = A\cos(st-kx), \quad u = -U\sin(st-kx) \quad (3)$$

where $U = sAL_w/H$, and $k = FU/(gA)$. In the above relations, U is the amplitude of tidal velocity, k is the tidal wave number, and $F = 8/(3\pi)\ c_dU/H$ is the coefficient of the leading term in the Fourier expansion of the friction term. By plugging these solutions into the mass and momentum equations,

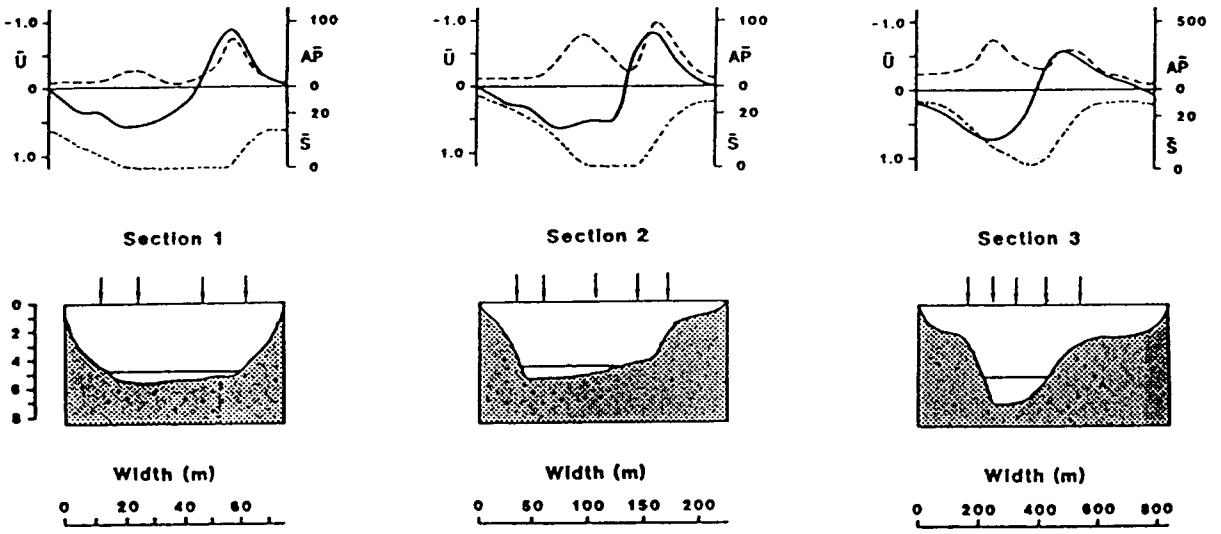

Figure 3. Sectionally-averaged velocity (—, m/s), sediment load (- - -, ppt m^2) and salinity (·–·, ppt) over individual tidal cycles in 1982 along with transverse topography at sections 1 (25 May, Q = 3.6 m^3/s), 2 (27 April, Q = 5.9 m^3/s) and 3 (26 Feb., Q = 25.9 m^3/s) along the River Tamar. Cross-sections show station positions, depths below high water spring tide, and the level of spring tide low water. Adapted from Uncles et al. (1985).

one finds that these solutions hold at lowest order only if the following parameters are $O(\varepsilon) << 1$:

$$A/H,\ h/H,\ kL_w,\ s/F,\ A_2/A,\ u_{river}/U \quad (4)$$

where $u_{river} = Q/(Hw)$. Unlike F&A94, here we do not explicitly consider the effect of time-varying estuary width due to the presence of intertidal flats or marsh.

The very simple solutions given by (3) result at lowest order largely because along-channel gradients in channel width dominate velocity gradients in the mass equation, and the friction term dominates acceleration in the momentum equation (F&A94). This is in contrast to the classical solution associated with the phase speed $(gH)^{1/2}$, which assumes precisely the opposite scaling. The $O(\varepsilon)$ terms, in the order listed in (4), are due to: (i) finite tidal amplitude, (ii) variations in tidally averaged channel depth, (iii) velocity gradients due to wave propagation, (iv) local acceleration, (v) external overtide forcing, and (vi) river discharge.

For spring tide along the Tamar (Uncles et al. 1985), the effective amplitude to depth ratio applicable to the nonlinear friction and continuity terms in (1)-(2) is $\frac{1}{2}(H_{high}-H_{low})/H_{midtide} \approx 0.6$ at spring tide, which is significantly less than $A/H_{midtide} \approx 1$ (Table 1). This is because the channel banks in the River Tamar are sloped such that the average depth at high water, H_{high}, is significantly less than $H_{low} + 2A$ (Figure 3). Alternatively, one could include tidal flats in the hydrodynamic equations, formulated such that they transported no momentum and their width varied over the tidal cycle (F&A94). However, such an approach would significantly complicate the formulation of sediment transport. The River Tamar is sufficiently narrow that it is probably reasonable to allow momentum transport over the entire cross-section, including intertidal areas. Thus from this point forward, hydrodynamic contributions resulting from the nonlinear friction and nonlinear continuity terms will be scaled by A_{eff}/H, where $A_{eff} = (H_{high}-H_{low})/2$ is the "effective" amplitude. (Note that U remains sAL_w/H, where A is the actual tidal amplitude.)

The remaining parameters in (4) are all significantly less than A_{eff}/H, with the exception of u_{river}/U in the most landward portion of the River Tamar (Table 1). As we will see, the ebb dominance favored by u_{river} in the upper reaches of the estuary is fundamental in establishing a stable turbidity maximum and an equilibrium budget for suspended sediment. A relatively substantial river discharge of Q = 10 m^3/s gives $u_{river}/U = Q\exp(x/L_w)/(w_0HU) \le A_{eff}/H$ for $x \le$ 19.6 km, which encompasses 93% of the Tamar estuary. Expressed somewhat differently, the scaling applied here, which assumes $\varepsilon \le O(A_{eff}/H)$ is valid only for

$$x \le L_w \log\left\{\left(A_{eff}/H\right)\left(w_0HU/Q\right)\right\} \quad (5)$$

A more stringent limitation on the applicability of this analysis to the River Tamar under most conditions is probably the presence of the tidal weir

at x = 21 km. In reality, a reflected tidal wave is generated at this point which propagates seaward along the estuary for a distance on the order of L_w before being dissipated by the combined effects of rapid channel expansion and strong bottom friction.

1.2 Higher order solution, surface elevation

If we follow a formal perturbation analysis and define

$$\eta = A\left\{\eta_0 + \varepsilon\eta_1 + O\left(\varepsilon^2\right)\right\} \tag{6a}$$

$$u = A\left\{u_0 + \varepsilon u_1 + O\left(\varepsilon^2\right)\right\} \tag{6b}$$

such that $\varepsilon << 1$, then $\eta_0 = \cos(st\text{-}kx)$ and $u_0 = -\sin(st\text{-}kx)$. Substitution of these solutions into the mass and momentum equations, and grouping of $O(\varepsilon)$ terms eventually yields $\varepsilon\eta_1 = \varepsilon\eta_{10} + \varepsilon\eta_{11} + \varepsilon\eta_{12}$ where

$$\varepsilon\eta_{10} = \frac{kL_w u_{river}}{U} \tag{7a}$$

$$\varepsilon\eta_{11} = \left(\frac{s}{F} - kL_w\right)kx\cos(st - kx) + 2\frac{h}{H}kx\sin(st - kx) \tag{7b}$$

$$\varepsilon\eta_{12} = -\frac{A_{eff}}{H}kx\sin(2st - 2kx) + \frac{A_2}{A}\cos\left(2st - 2kx - \theta_2\right) \tag{7c}$$

The first subscript indicates the terms are $O(\varepsilon^1)$, while the second subscript on each component indicates the frequency relative to s. Thus η_0 and u_0 are also equal to η_{01} and u_{01}. In deriving (7) it is important to note that although $kL_w << 1$, kx can be $O(1)$, since x can be much greater than L_w.

In (7), $\varepsilon\eta_{10}$ provides the mean pressure gradient needed to drive a spatially-invariant river discharge seaward. Because η_0 and u_0 are 90° out of phase, at $O(\varepsilon)$ there is no set-up induced by Stokes drift. $\varepsilon\eta_{11}$ represents the competition between friction and channel convergence in dampening or focusing tidal amplitude. If friction is strong (large F) and convergence weak (large L_w and/or locally negative h), then amplitude decreases landward along channel. Conversely, if convergence overcomes friction, amplitude increases. $\varepsilon\eta_{12}$ contains internally generated and externally forced contributions to the overtide. Together, η_0 and the first term in (7c) produce a tide which is faster rising than falling and, by continuity, flood dominant. Conceptually, the tide is faster rising because the crest of the tide propagates more quickly than the trough (because s/k ~ channel depth). Over a significant distance, the crest begins to "catch up" with the trough, decreasing the duration of the intervening flood.

Neglecting $O(\varepsilon^2)$, (7c) and the first term in (7b) are consistent with F&A94. However, F&A94 did not include river flow nor along-channel depth variation, two contributions which can be important when considering the equilibrium sediment budget or when exploring implications for morphodynamic evolution. As in F&A94, we have included nonlinearities generated by the depth variation in the friction term, but we have not included the third harmonic generated by quadratic friction. The reasoning behind this is two-fold: (i) quadratic friction appears to do a poor job reproducing observations of the third harmonic in natural tidal estuaries (e.g., Prandle 1980; Friedrichs & Madsen 1992); (ii) in general, the third harmonic does not contribute strongly to net sediment transport. This approach is equivalent to setting the $c_d|u|$ contribution in (1) to exactly $8/(3\pi)$ $c_d U$ before expanding (1).

1.3 Higher order solution, velocity

By substituting (6)-(7) into continuity (or momentum), we find that to $O(\varepsilon)$, $\varepsilon u_1 = \varepsilon u_{10} + \varepsilon u_{11} + \varepsilon u_{12}$ where

$$\varepsilon u_{10} = -\frac{u_{river}}{U} \tag{8a}$$

$$\varepsilon u_{11} = \left\{\left(kL_w - \frac{s}{F}\right)kx - \frac{h}{H}\right\}\sin(st - kx) + \left(2\frac{h}{H}kx + kL_w\right)\cos(st - kx) \tag{8b}$$

$$\varepsilon u_{12} = \frac{1}{2}\frac{A_{eff}}{H}\sin(2st - 2kx) - 2\frac{A_{eff}}{H}kx\cos(2st - 2kx) - 2\frac{A_2}{A}\sin\left(2st - 2kx - \theta_2\right) \tag{8c}$$

Eq. (8) reduces to the no tidal flat case considered by A&F94 when $u_{river} = h/H = 0$ and $A_{eff} = A$. However there is a typographical error in the solution of

A&F94: the first line of their (35) should read $U/2$ $\{(\varepsilon_h-\varepsilon_b)\sin(2st-2kx) - 2\gamma kx\cos(2st-2kx)\}$.

In (8), εu_{10} is the velocity associated with the spatially invariant river discharge. The portions of εu_{11} proportional to kx represent the along-channel growth or decay in velocity amplitude paralleling the along-channel variation in $\varepsilon\eta_{11}$. The remaining terms in εu_{11} arise from applying the higher order linear continuity terms to η_0. In particular, the $kL_w\cos(st-kx)$ term in (8b) causes the phase difference between u and η to decrease as the rate of along-channel convergence decreases. Together, u_0 and the second term in εu_{12} produce a flood dominant current which is a central control on the sediment budget in funnel-shaped tidal estuaries. The third term in (8c) can also contribute significantly to ebb- or flood dominant currents depending on the relative phase between η_0 and η_{12} at the mouth of the estuary. The first term in εu_{12} arises from applying the higher order nonlinear continuity terms to η_0 and does not contribute significantly to net sediment transport.

In tidal estuaries significantly deeper than the Tamar, mean gravitational circulation can produce landward directed near bottom currents which can contribute to net sediment transport (e.g., Nichols & Poor 1967). An estimate of the strength of gravitational circulation is given by the Officer's (1976) solution derived from a balance between the mean pressure gradient and friction in a channel of rectangular cross-section:

$$u_{grav} = \frac{\partial\rho}{\partial x}\frac{gH^3}{48\rho_0 A_v}\left\{1-9\left(\frac{z}{H}\right)^2-8\left(\frac{z}{H}\right)^3\right\} \quad (9)$$

In deriving (9), eddy viscosity (A_v) and density gradient ($\partial\rho/\partial x$) are assumed independent of z, ρ_0 is depth averaged density, and the boundary conditions are $\partial u_{grav}/\partial z = 0$ at $z = 0$, $u_{grav} = 0$ at $z = -H$, and $\int u_{grav}dz = 0$ integrated over the water column. With $H = 2.5$ m, a conservatively large $\partial\rho/\partial x = 2$ kg/m^3 per km, and a conservatively small $A_v = 10^{-3}$ m^2/s, we find $u_{grav}/U < 0.01$, yielding u_{grav} insignificant in the Tamar compared to tidal asymmetries or river flow in the upper reaches of the estuary near the turbidity maximum.

1.4 Comparison to observations from River Tamar

Figure 4 compares the predictions of (6)-(8) to observations from the River Tamar collected by George (1975) and Uncles et al. (1985). The only parameter "tuned" in the analytical solution is the friction coefficient, which was chosen to give the best least-squares fit between observed and modeled along-channel propagation in tidal phase in Figure 4(a). The geometric and forcing parameters applied in the model, along with the size of the small parameters in (4) are given in Table 1. Observations of surface elevation along the Tamar were taken simultaneously over a single semi-diurnal spring tide on 14 October 1970 (George 1975); observations of cross-sectionally averaged velocity at spring tide (see Figure 3) are not synoptic (Uncles et al. 1985). The observations of surface elevation as well as velocity at sections 1 and 2 were taken at times of minimal freshwater discharge, thus the analytical solutions in Figure 4 do not incorporate η_{10} or u_{10}; they also do not include the effect of h/H.

The analytical solution captures the slight increase in high tide elevation and maximum current velocity seen as one moves landward along the estuary. The

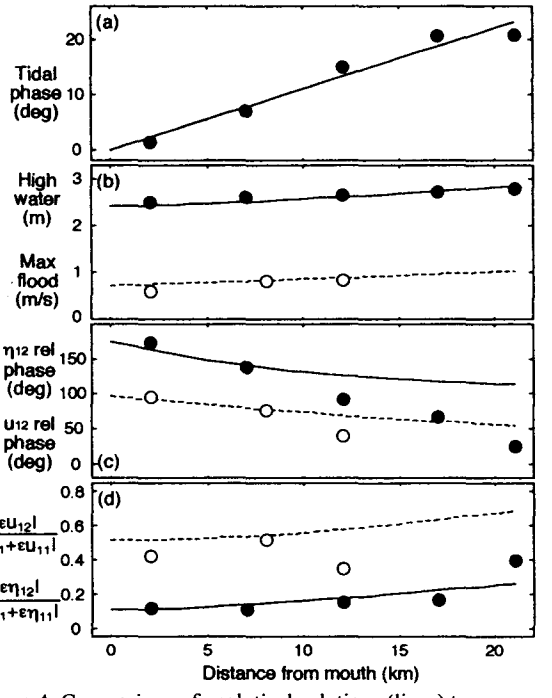

Figure 4. Comparison of analytical solutions (lines) to observations (circles) for the River Tamar. Solid lines and filled circles refer to elevation, dashed lines and open circles refer to cross-sectionally averaged velocity: (a) phase of semi-diurnal component relative to mouth; (b) maximum tidal elevation (relative to mid-tide at the mouth) and maximum flood velocity; (c) phase of overtide relative to semi-diurnal component; (d) amplitude of overtide relative to semi-diurnal component. Observations from George (1975) and Uncles et al. (1985).

analytic solution also predicts the right order of magnitude for the quarter-diurnal components (η_{12} and u_{12}), with the amplitude ratio for quarter-diurnal velocity being two to three times that for elevation. The behavior of the quarter-diurnal relative phase is reproduced well over the seaward portion of the estuary, and the generally faster-rising and flood dominant nature of the tide is captured throughout the system. The phase, θ_{xn}, of a given component is determined by re-expressing that component as $|\eta_{xn}|\cos(nst-\theta_{xn})$. The relative phase of η_{12} is then defined as two times the relative phase of $\eta_0+\varepsilon\eta_{10}$ minus the phase of η_{12}. The relative phase of u_{12} is analogously defined with respect to $u_0 + \varepsilon u_{10}$.

The analytical solution significantly under-predicts the decrease in quarter-diurnal relative phase of the surface tide observed toward the inner portion of the estuary. This is because the tidal elevation curve is kinematically truncated in the innermost Tamar by the elevation of the channel bottom (George 1975), a process which is not represented in the dynamics of (6)-(8). Truncation of the tidal curve around low water can significantly reduce the quarter-diurnal relative phase determined by harmonic analysis (Speer et al. 1991). One should expect kinematic truncation to affect velocity asymmetry less, since maximum flood and ebb occur outside the period of truncation.

2. SEDIMENT DYNAMICS

2.1 Lowest order solution

To calculate suspended sediment concentration, we start with the one dimensional advection-dispersion equation applied by S&S96 to a constant width channel and adapt it here for a channel with varying width:

$$\frac{\partial C}{\partial t}+\frac{1}{w}\frac{\partial}{\partial x}(wuC) - \frac{1}{w}\frac{\partial}{\partial x}\left(wK\frac{\partial C}{\partial x}\right) = E - D \qquad (10)$$

In (10), C is depth-integrated suspended sediment concentration, K is the longitudinal dispersion coefficient, $E = (\alpha/T_c)u^2$ is the erosion rate, and $D = C/T_c$ is the deposition rate. α is a spatially varying empirical coefficient parameterizing the ease with which bottom sediment can be mobilized, and T_c is the adjustment time-scale for the concentration field, assumed to be constant for a given type of suspended sediment. In truth, deposition is not proportional to depth-integrated suspended sediment concentration; it is more closely proportional to near-bed suspended sediment concentration. To reconcile this, we will assume that nearly all of the suspended sediment remains in the lower part of the water column and is not vertically spread or concentrated by tidal oscillations in water depth. Then depth-integrated concentration remains roughly proportional to near-bed concentration. As long as the sediment response time is significantly less than the tidal time scale, this is not an unreasonable assumption.

The above formulations for E and D allow simultaneous erosion and deposition. Mathematical models for sediment transport of fine sediment often assume that erosion occurs only when bottom stress, τ, is greater than some critical level, τ_e, and that deposition only occurs for $\tau < \tau_d$, where τ_d is the critical deposition shear stress (e.g., Dyer 1986). This formulation is based on laboratory observations of flow over cohesive sediments. Since it is generally observed in the laboratory that $\tau_d < \tau_e$, this formulation has been termed exclusive erosion and deposition. However, more recent observations under field conditions in estuaries containing cohesive sediment suggest that erosion and deposition can occur simultaneously in real estuaries (e.g., Sanford & Halka 1993). This disagreement with laboratory observations may be due to the larger scales present in the field which produce greater heterogeneities in terms of sediment properties and turbulence over scales of 10's to 100's of meters. When these heterogeneities are integrated into simple mathematical models, it appears that a bottom boundary which allows simultaneous erosion and deposition better represents the behavior of estuarine sediment in situ (Sanford & Halka 1993). This is a convenient result, for allowing erosion and deposition to occur together is easier to model analytically.

If a lowest order balance in (10) is assumed between erosion and deposition, then the concentration scale is given by $C_m = \alpha_m U^2$, where α_m is the scale of $\alpha(x)$. Scaling t by 1/s, u by U, and x by L_w, the orders relative to erosion and deposition of the three terms on the left hand side of the concentration equation (local change, advection, dispersion) are, respectively:

$$\varepsilon_T = sT_c, \quad \varepsilon_U = \frac{\varepsilon_T U}{sL_w}, \quad \varepsilon_U\varepsilon_D^2 = \frac{\varepsilon_U K}{L_w U} \qquad (11)$$

For spring tide along the River Tamar, T_c can be estimated by examining the time-lag between depth-integrated suspended sediment concentration and cross-sectionally averaged velocity. These difficult observations were obtained successfully by Uncles et al. (1985) and are displayed in Figures 3 and 5. For $T_c = 0$, one would expect $|u|$ to be exactly in phase with C. From the observations of Uncles et al. (1985), it appears that ~30 min $\leq T_c \leq$ ~60 min (Figure 5). The sediment response time can be expected to be about equal to the vertical distance which scales the fall off of sediment concentration divided by the suspended sediment fall velocity. If the vertical scale for sediment concentration is about a meter, then $T_c \approx$ 30-60 min corresponds to a fall velocity of about 0.4 mm/s which, in turn, is characteristic of medium silt (e.g., Dyer 1986).

A sediment response time of 30 to 60 minutes gives ~0.3 $\leq sT_c \leq$ ~0.6, which is less than or equal to A_{eff}/H, the largest parameter neglected at lowest order in the hydrodynamic solution. With $U \approx 0.7$ m/s and $L_w \approx 5$ km, we find $U/(sL_w) \approx 1$ for the Tamar, and $\varepsilon_T \approx \varepsilon_U$. This scaling is in contrast to S&S96 who, for constant width channels, treated sT_c as $O(1)$ and assumed advection in the concentration equation to be much less important than $\partial C/\partial t$. Along funnel-shaped estuaries, however, advection of suspended sediment is more important than advection of momentum because the length (L_w) which scales gradients in sediment concentration is much less than the length ($1/k$) which scales gradients in along-channel velocity.

The ratio scaling the importance of dispersion relative to advection is given by $\varepsilon_D^2 = K/(L_w U)$. If one assumes the intra-tidal dispersion coefficient $K < 100$ m^2/s (e.g., Fischer et al. 1979; Zimmerman 1986), then for the River Tamar, $K/(L_w U) < 0.03$, which suggests that the contribution of dispersion is not very important. For tidally averaged equations applied to estuaries with irregular geometries, K may be $O(1000)$ m^2/s because the effects of periodic tidal advection are incorporated into "dispersion" (e.g., Zimmerman 1986). Here we treat tidal advection separately, and the appropriate intra-tidal K is much smaller.

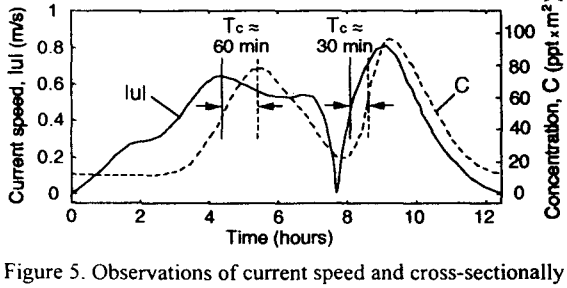

Figure 5. Observations of current speed and cross-sectionally integrated suspended particle concentration over a spring tidal cycle. Estimates of the time-lag between current speed and concentration are also shown. Modified from Uncles et al. (1985).

Defining $C = C_m\{C_0 + \varepsilon C_1 + O(\varepsilon_2)\}$, it follows from the lowest order relation, $E \approx D$, that

$$C_0 = \alpha' u_0^2 = \frac{\alpha'}{2}\{1 - \cos 2(st - kx)\} \qquad (12)$$

where $\alpha' = \alpha/\alpha_m$. From Figures 3 and 5, we can see that (12) at least qualitatively resembles the observations of cross-sectionally integrated sediment concentration collected by Uncles et al. (1985).

It is worth noting that as sT_c goes to zero, $E = D$ exactly, and $C = \alpha u^2$ exactly. Then instantaneous sediment transport is given by αu^3, which is very much like the classic Meyer-Peter and Müller (1948) formula for bedload sediment transport. Thus the analytical theory for tidal sediment concentration and transport presented here can easily be extended to bedload, namely the regime for which sT_c is exceedingly small.

2.2 *Higher order solution*

Substitution into the concentration equation and grouping of $O(\varepsilon)$ terms yields the following equation for C_1:

$$\varepsilon C_1 = 2\alpha' \varepsilon u_1 u_0 - sT_c \frac{\partial C_0}{\partial t'} - \frac{T_c U}{L_w} e^{x'} \frac{\partial}{\partial x'}\left(e^{-x'} u_0 C_0\right) \qquad (13)$$

where $t' = st$ and $x' = x/L$. The higher order sources of concentration in (13) include altered erosion patterns brought about by the presence of u_1 interacting with u_0, the finite time it takes for the concentration to reach an equilibrium between erosion and deposition, and along channel advection of the concentration field. The latter two effects together are often attributed to settling and scour lag (e.g., Postma 1967). Note that dispersion does not appear in the equation for C_1 because dispersion is two orders of ε smaller than advection in the concentration equation.

Applying the known expressions for C_0, u_0 and u_1 then gives us $\varepsilon C_1 = \varepsilon C_{10} + \varepsilon C_{11} + \varepsilon C_{12} + \varepsilon C_{13}$ where

$$\frac{\varepsilon C_{10}}{\alpha'} = \left(\frac{s}{F} - kL_w\right)kx + \frac{h}{H} \tag{14a}$$

$$\frac{\varepsilon C_{11}}{\alpha'} = \left\{\frac{3}{4}\frac{T_c U}{L_w}\frac{1}{w\alpha'}\frac{d(w\alpha')}{dx'} + \frac{2u_{river}}{U} - \frac{2A_{eff}}{H}kx + \frac{2A_2}{A}\sin\theta_2\right\}\sin(st-kx) - \left\{\frac{A_{eff}}{2H}kx - \frac{2A_2}{A}\cos\theta_2\right\}\cos(st-kx) \tag{14b}$$

$$\frac{\varepsilon C_{12}}{\alpha'} = -\left(kL_w + sT_c + \frac{2h}{H}\right)\sin(2st-2kx) - \frac{1}{2}\left\{\left(\frac{s}{F} - kL_w\right)kx + \frac{h}{H}\right\}\cdot \cos(2st-2kx) \tag{14c}$$

$$\frac{\varepsilon C_{13}}{\alpha'} = -\left\{\frac{1}{4}\frac{T_c U}{L_w}\frac{1}{w\alpha'}\frac{d(w\alpha')}{dx'} - \frac{2A_{eff}}{H}kx + \frac{2A_2}{A}\sin\theta_2\right\}\sin(3st-3kx) - \frac{2A_2}{A}\cos\theta_2\cos(3st-3kx) \tag{14d}$$

Of all the terms in C_1, only the sine portion of C_{11} will contribute to tidally averaged sediment transport at leading order, because only it is correlated with u_0. The first term in the sin(st-kx) component of (14b) originates from tidal advection in (13) (a component of settling lag/scour lag), while the remaining three are due to altered erosion arising from the interaction of u_1 and u_0.

The equation for net sediment flux over a tidal cycle, S, is net advection minus net dispersion:

$$S = \langle uC\rangle - \langle K\frac{\partial C}{\partial x}\rangle \tag{15}$$

where $\langle\ \rangle$ indicates a tidal average. Keeping the leading order contributions to S due to advection and dispersion, (15) can be re-expressed as

$$S \approx UC_m\left\{\langle u_0C_0\rangle + \varepsilon\langle u_1C_0\rangle + \varepsilon\langle u_0C_1\rangle + \varepsilon_D^2\langle\partial C_0/\partial x'\rangle\right\} \tag{16}$$

We have included the $O(\varepsilon)$ advection terms because $\langle u_0C_0\rangle = 0$. The dispersion term involving C_0 is non-zero, so dispersion is an order of ε more important in the sediment transport equation than it is in the concentration equation. Even so, for funnel-shaped estuaries comparable to the Tamar, the leading order dispersion term is still $O(\varepsilon_D^2) << O(\varepsilon)$. Thus we may still neglect dispersion. This result is in contrast to S&S96, who showed that for constant width basins about 20 km long, with relatively weak tides ($A/H \approx 0.15$) and coarse sediment ($sT_c \approx 0.04$), advection and dispersion can be of equal importance in contributing to tidally averaged sediment transport. In such systems, net transport due to advection relative to dispersion is scaled by $(L^2s/K)(sT_c)(A/H)^2$, where L is the length of the tidal estuary.

The solution for S is more compact than that for u_1 or C_1 because relatively few terms survive time averaging. In u_1, only u_{10} and the cos(2st-2kx) portion of u_{12} are correlated with C_0, and in C_1, only the sin(st-kx) portion of C_{11} is correlated with u_0. Plugging in the solutions for u_0, u_1, C_0 and C_1 into (16) and averaging yields contributions (in order) from river flow, tidal asymmetry and settling/scour lag:

$$S = \frac{3}{2}UC_m\alpha'\left\{-\frac{u_{river}}{U} + \left(\frac{A_{eff}}{H}kx - \frac{A_2}{A}\sin\theta_2\right) - \frac{1}{4}\frac{T_cU}{L_w}\frac{1}{w\alpha'}\frac{d(w\alpha')}{dx'}\right\} \tag{17}$$

River flow transports sediment seaward; internally generated tidal asymmetry transports sediment landward; externally forced tidal asymmetry and settling lag/scour lag can transport sediment landward or seaward, depending on the phase of the externally forced overtide and the spatial structure of bed erodability, α'.

With α' constant, (17) becomes

$$S = \frac{3}{2}UC_m\alpha'\left\{-\frac{u_{river}}{U} + \frac{A_{eff}}{H}kx - \frac{A_2}{A}\sin\theta_2 + \frac{1}{4}\frac{T_cU}{L_w}\right\} \tag{18}$$

With $d\alpha'/dx = 0$, net landward sediment transport by settling/scour lag occurs because of strong along channel width convergence, a newly recognized interaction capable of helping maintain the turbidity maximum. Classically, settling/scour lag moves sediment towards areas of lower velocity (Postma 1967). Here, spatial gradients in velocity are minimal, and settling/scour lag acts to move sediment toward areas of increasingly narrow

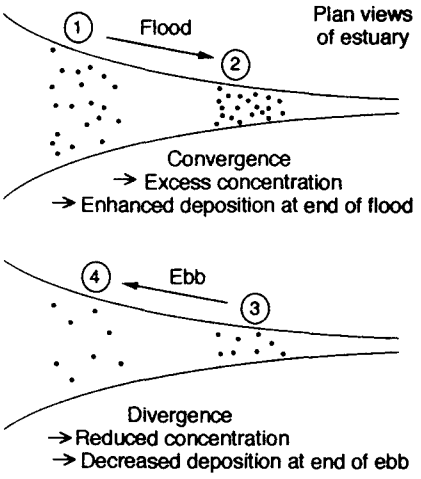

Figure 6. Illustration of net landward suspended sediment transport due to settling/scour lag interacting with width convergence.

channel width. Figure 6 shows conceptually how settling/scour lag is effective in a funnel-shaped tidal estuary with uniform bed erodability.

During flood, sediment is moved from a wider portion of the estuary toward a narrower portion. Because of settling/scour lag, sediment concentration does not respond instantaneously to the strength of the local velocity. Thus a given parcel of suspended sediment becomes crowded over a smaller patch of channel bottom. There is now an excess concentration relative to the equilibrium value supported by erosion, and enhanced deposition occurs toward the end of flood. During ebb the opposite process occurs. A given parcel of suspended sediment is spread over an increasingly wider area of the estuary. The reduced concentration relative to the value supported by erosion results in decreased deposition toward the end of ebb.

It may seem strange that local sediment concentration increases with along-channel width convergence when the concentration of the incompressible water carrying the sediment clearly does not. This is because water responds to convergence of channel width by moving upwards, and the tide rises during flood. Sediment dynamics are not affected by the rise of the sea surface because it is assumed that depth-integrated (rather than depth-averaged) sediment concentration controls the deposition rate. As discussed in Section 2.1, this assumption makes sense if most of the suspended sediment remains in the lower part of the water column.

One contribution to higher order hydrodynamics which conspicuously does not contribute to tidally averaged sediment transport is h/H, i.e., perturbations in along-channel depth away from the mean depth of the entire estuary. The only velocity component affected by perturbations in depth is u_{11}, which is uncorrelated with C_0. The altered erosion patterns due to the interaction of u_{11} and u_0 contribute to C_{10} and C_{12}, but neither of these is correlated with u_0. Thus if depth perturbations along a shallow funnel-shaped estuary are characterized by $h/H \leq O(A_{eff}/H)$ (as is the case for many macro-tidal estuaries), then the nature of the equilibrium suspended sediment budget is not related at lowest order to along-channel variation in depth. This was initially a surprising result, for this work, as an extension of S&S96, anticipated determining the along-channel variation in h/H required to satisfy a zero along-channel gradient in cross-sectionally integrated sediment transport. Instead, this study has shown that h/H plays no significant role in the equilibrium sediment budget in such systems.

3. HIGH TURBIDITY REGION

3.1 Along-channel location

Still assuming the bed erodability to be independent of x, (18) can be solved easily to find the location of along-channel convergence of sediment transport. Figure 7 schematically displays the contributions to tidally averaged sediment transport of (i) river flow, (ii) internally generated tidal asymmetry (i.e., flood dominance), and (iii) settling/scour lag associated with width convergence, all as a function of position along the estuary. Unless sediment transport due to external tidal asymmetry is large and directed seaward, sediment transport at the estuary mouth will be landward due to the interaction of channel convergence with settling/scour lag. (For the Tamar $\theta_2 \approx 175°$, minimizing the net effect of the external overtide.) As one moves landward, the magnitude of landward transport by flood dominance and seaward transport by river flow both increase. Initially the linear increase in flood dominance with distance is more rapid than the exponential increase in river flow, and net sediment transport is landward. But eventually seaward sediment transport by river flow overcomes the combined effect of landward transport by flood dominance and settling/scour lag.

Figure 8 displays observations of suspended particulate matter at spring high water (ranges > 4 m) along the Tamar estuary during 1985 as reported by Uncles and Stephens (1989). The concentration profiles have been normalized by tidal amplitude squared in an attempt to reduce the effect

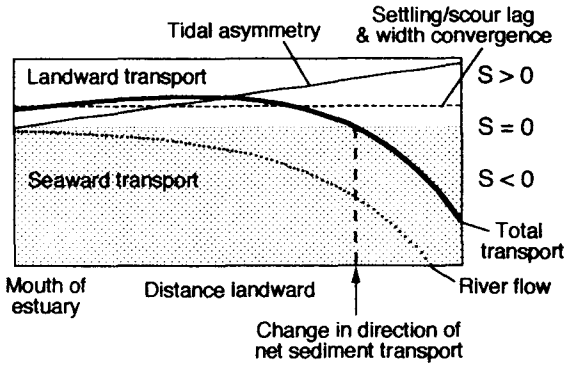

Figure 7. Contributions to tidally averaged sediment transport as a function distance along a shallow, funnel-shaped estuary. This scenario assumes (i) bed erodability is independent of along channel position and (ii) asymmetries present at the mouth do not contribute significantly to net sediment transport.

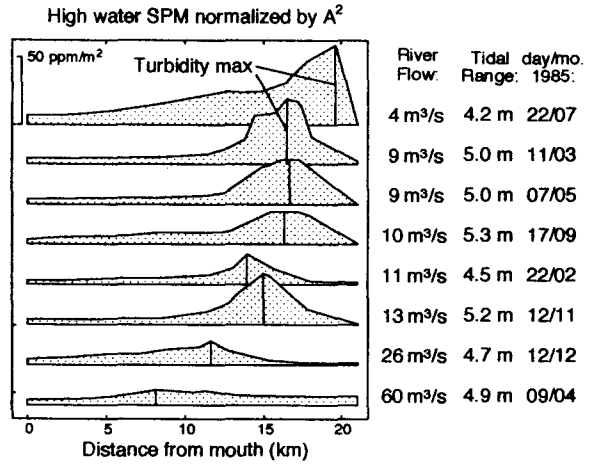

Figure 8. Observations of suspended particulate matter at spring high water along the River Tamar during 1985, normalized by tidal amplitude squared and arranged in order of increasing river discharge (modified from Uncles & Stephens 1989).

of differences in peak tidal velocity from one spring tide to the next. Furthermore, they have been displayed from top to bottom in order of increasing fresh water discharge. Two distinct patterns can be seen in the data in response to increasing Q: (i) the high turbidity region moves seaward; and (ii) the turbidity maximum becomes less intense.

Figure 9(a) compares the observed location of the turbidity maximum in Figure 8 with the prediction of (18) for the convergence point of along-channel net sediment transport. The positions for the turbidity maximum predicted by the analytical solution are reasonably consistent with the observations. (They are also well seaward of the

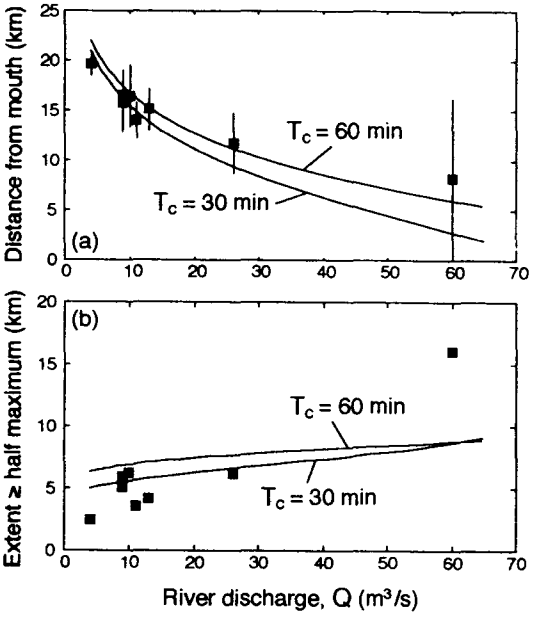

Figure 9. Observed and predicted properties of the high turbidity region along the River Tamar as a function of river discharge: (a) Along-channel location of the turbidity maximum; (b) along-channel extent of concentrations greater than or equal to one half the turbidity maximum. In (a), vertical bars are along-channel extent centered about the turbidity maximum. (Observations from Uncles & Stephens 1989.)

high u_{river} limit given by (5)). The theory also predicts the observed migration of the turbidity maximum toward the mouth of the estuary as river discharge increases. As the turbidity maximum migrates seaward, the magnitude of net landward transport by the tides decreases linearly. In contrast, net seaward transport by the river decreases exponentially. Thus a little closer to the mouth, a slightly less effective tidal asymmetry can balance net transport by a much greater river discharge because u_{river} is significantly diminished by an exponentially increased channel width.

3.2 Equilibrium along-channel extent

Although the above analysis appears to identify the location of the turbidity maximum, it does not represent an equilibrium sediment budget (i.e., zero gradient in cross-sectionally integrated, tidally averaged sediment transport). Clearly if bed erodability is uniform in space, rapid deposition will occur in the vicinity of the turbidity maximum, and a continual sink for suspended sediment will exist. Continual deposition will eventually create a positive perturbation in bottom elevation at this

location. However the sediment transport solution indicates that a perturbation of size $h/H \leq O(A_{eff}/H)$ does not contribute to the leading order sediment budget. So with uniform α' and $h/H \leq O(A_{eff}/H)$, no feedback can occur which could lead to a stable morphology. It seems that the only way to produce an equilibrium sediment budget at leading order is to allow α' to vary in x. An alternative explanation might be that $d\alpha'/dx = 0$, and funnel-shaped macrotidal estuaries such as the Tamar are very far from morphodynamic equilibrium. Considering the highly energetic conditions, high sediment concentrations present and stable tidal forcing, this alternative hypothesis is dismissed.

To solve for the along-channel distribution of α' at equilibrium, we assume that the rate of new sediment input from the ocean and/or river is negligible relative to the amount of suspended sediment instantaneously in motion in the vicinity of the turbidity maximum, and we also neglect the externally forced overtide. Then the equilibrium sediment budget will be nearly equivalent to the following condition that $S \approx 0$ everywhere:

$$-\frac{u_{river}}{U} + \frac{A_{eff}}{H} kx - \frac{1}{4}\frac{T_c U}{L_w}\frac{1}{w\alpha'}\frac{d(w\alpha')}{dx'} = 0 \quad (19)$$

Expanding u_{river} about its value at x_{turb}, and solving for α' then yields

$$\alpha' \approx \exp\left(-\frac{2u_{river}(x_{turb})}{U^2 T_c L_w}(x - x_{turb})^2\right) \quad (20)$$

which is strictly valid only for $x - x_{turb} << L_w$.

Figure 9(b) compares the observed along-channel extent of the region of high turbidity in Figure 8 with that predicted by (20). Along-channel extent is defined here as the length of channel containing sediment concentrations greater than or equal to half the concentration observed at the turbidity maximum. The analytical solution reproduces the observed increase in along-channel extent with increased river discharge. Except for the minimum and maximum discharge cases, (20) also does a reasonable job of quantitatively predicting the observed extent of the high turbidity region. The observed extent for the lowest discharge case is probably limited by its proximity to the weir present 21 km from the mouth. Conversely, the low sediment concentrations associated with the highest discharge may have blurred its signal into the background concentration of very low density matter not associated with resuspension, thus exaggerating the along-channel extent of the high turbidity region.

3.3 Migration of finite sediment supply

As shown in the previous section, an equilibrium sediment budget requires the region of high bed erodability (i.e., the region of large α') to migrate seaward with increased river discharge. This suggests that the region of high turbidity is formed from a mobile pool of easily erodable sediment. Furthermore, the supply appears to be finite, for after the source material has migrated to a new area, very

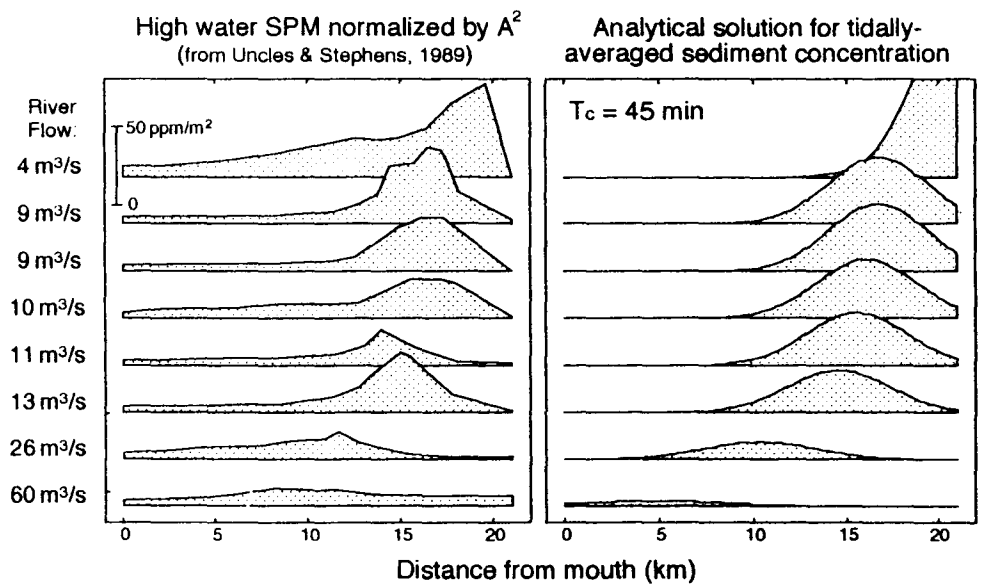

Figure 10. Observed and predicted suspended sediment concentration profiles along the Tamar, normalized by tidal amplitude squared and arranged in order of increasing river discharge (observations from Uncles & Stephens 1989).

low values for α' are found away from the new turbidity maximum, which suggests the process of migration does not leave behind much excess unconsolidated bed material. If the total pool of easily mobilized sediment is approximately constant for a typical spring tide, then the product of its along-channel extent times the intensity of the turbidity maximum times the channel width at x_{turb} should remain roughly fixed. Figure 9(b) indicates that the along-channel extent of the high turbidity region varies rather weakly in response to river discharge (except for Q = 4 and 60 m^3/s, as discussed above). Therefore the total pool ~ $C_m w(x_{turb})$, and the scale of the turbidity maximum should vary with x_{turb} as follows:

$$C_m \sim \frac{\text{Total pool}}{w(x_{turb})} \qquad (21)$$

Figure 10 compares observed profiles of the high turbidity region along the River Tamar with analytical solutions for identical river discharges by combining (i) the concentration scale predicted by (21), (ii) the shape and along-channel extent predicted by (20), and (iii) the position predicted by (18). An intermediate sediment response time scale of T_c = 45 min was chosen for the theoretical predictions. Comparison of the observed and predicted profiles still requires incorporation of an arbitrary constant in (21) good for all river discharges. (Note that there is no vertical scale on the analytical solutions in Figure 10.) Nonetheless, the analytical solution reasonably captures the along-axis position, along-channel extent and relative intensity of the region of high turbidity along the River Tamar.

The model results displayed in Figure 10 require the presence of a finite, mobile supply of easily erodable bed source material. Direct evidence of a rapidly moving fine-grained deposit along the River Tamar is provided by Uncles et al. (1996), who describes the seasonally migrating distribution of "mobile, unconsolidated, bed-source mud" (p.381).

Figure 11 displays the along-channel distribution of this muddy deposit as a function of river discharge. Migration of the bed source material appears to parallel the seasonal migration of the high turbidity region.

In the summer and fall, when Q is typically small, the unconsolidated bed source mud is found in the upper reaches of the estuary, while in the winter and spring, when Q is typically large, the unconsolidated mud is found further seaward.

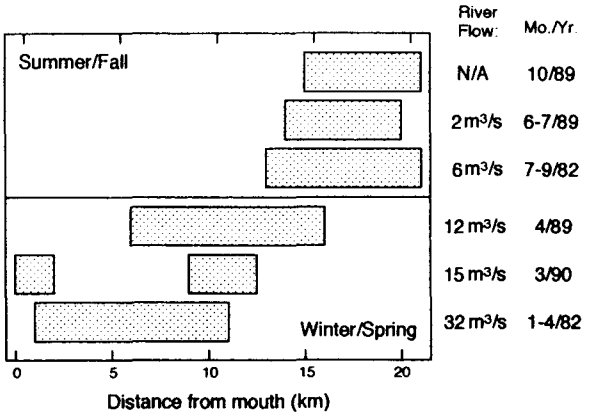

Figure 11. Observed distributions of mobile, unconsolidated bed-source mud along the River Tamar as a function of river discharge and season. Data from Uncles et al. (1996) and Bale et al. (1985).

Table 1. Morphological and tidal properties of the River Tamar.

Parameter	Value.	Stand. err
Distance from mouth to weir head	21 km	n.a.
H = average cross-section depth at midtide	2.4 m	0.1 m
h = 2½ x standard deviation of H	0.19 m	n.a.
A = spring tidal amplitude (from Fig 8)	2.4 m	0.1 m
$A_{eff}/H = ½(H_{high}-H_{low})/H_{midtide}$	0.60 m	0.1 m
L_w = e-folding length for width at midtide	4.7 km	0.8 km
w_0 = exponential fit for width at x = 0	650 m	200 m
$2\pi/k$ = tidal wave length fit to tidal phase	360 km	50 km
A_2/A = relative amplitude of overtide at mouth	0.11	n.a.
θ_2 = overtide relative phase at mouth	175°	n.a.
s/F = acceleration relative to friction	0.20	0.04
kL_w = width change relative to tide	0.09	0.02
u_{river}/U for seaward 93% of Tamar with Q = 10 m^3/s	≤ 0.6	n.a.
sT_c = sediment response time rel to tide	0.3-0.6	n.a.
$k/(L_wU)$ = dispersion relative to advection	0.03	n.a.

n.a. = not available or not applicable

ACKNOWLEDGMENTS

This work was funded in part by the U.S. Office of Naval Research, Harbor Processes Program, under contract no. N00014-93-1-0986. In addition, this

analysis is partly based on work in the PACE-project, in the framework of the EU-sponsored Marine Science and Technology Program (MAST-III), under contract no. MAS3-CT95-0002. This paper is contribution No. 2096 of the Virginia Institute of Marine Science.

REFERENCES

Allen, G.P., J.C. Salomon, P. Bassoullet, Y. du Penhoat & C. de Grandpré 1980. *Effects of tides on mixing and suspended sediment transport in macrotidal estuaries*. Sedimentary Geology 26: 69-90.

Bale, A.J., A.W. Morris & R.J.M. Howland 1985. *Seasonal sediment movement in the Tamar Estuary*. Oceanologica Acta 8: 1-16.

Dyer, K.D. 1986. *Coastal and Estuarine Sediment Dynamics*. New York: Wiley.

Fischer, H.B., E.J. List, R.C.Y. Koy, J. Imberger & N.H. Brooks 1979. *Mixing in Inland and Coastal Waters*. New York: Academic Press.

Friedrichs, C.T. & D.G. Aubrey 1994. *Tidal propagation in strongly convergent channels*. J. Geophysical Res. 99: 3321-3336.

Friedrichs, C.T. & O.S. Madsen 1992. *Nonlinear diffusion of the tidal signal in frictionally dominated embayments*. J. Geophysical Res. 97: 5637-5650.

George, K.J. 1975. *The tides and tidal streams of the Tamar estuary*. Ph.D. thesis, University of London, 555 pp.

Meyer-Peter, E. & R. Müller 1948. *Formulas for bedload transport*. Proc. Int. Meet. Assoc. Hydraulic Res., Stockholm: 39-64.

Nichols, M. & G. Poor 1967. *Sediment transport in a coastal plain estuary*. ASCE J. Waterways Harbors 93: 83-95.

Officer, C.B. 1976. *Two dimensional density gradient flow*. In: Physical Oceanography of Estuaries (and Associated Coastal Waters): 125-129. New York: Wiley.

Postma, H. 1967. *Sediment transport and sedimentation in the estuarine environment*. In G.H. Lauff (ed.), Estuaries: 158-179. Washington, D.C.: Amer. Assoc. Advancement of Science.

Prandle, D. 1980. *Modelling of tidal barrier schemes: an analysis of the open-boundary problem by reference to AC circuit theory*. Estuarine Coastal Marine Sci. 11: 53-71.

Sanford, L.P. & J.P. Halka 1993. *Assessing the paradigm of mutually exclusive erosion and deposition of mud, with examples from upper Chesapeake Bay*. Marine Geology 114: 37-57.

Schuttelaars, H.M. & H.E. de Swart 1996. *An idealized long-term morphodynamic model of a tidal inlet*. European J. Mechanics, B/Fluids 15: 55-80.

Speer, P.E., D.G. Aubrey & C.T. Friedrichs 1991. *Nonlinear hydrodynamics of shallow tidal inlet/bay systems*. In B.B. Parker (ed.), Tidal Hydrodynamics: 321-339. New York: Wiley.

Uncles, R.J., R.C.A. Elliott & S.A. Weston 1985. *Lateral distributions of water, salt and sediment transport in a partly mixed estuary*. Proc. 19th Int. Coastal Engineering Conf.: 3067-3077, New York: American Society of Civil Engineering.

Uncles, R.J. & J.A. Stephens 1989. *Distributions of suspended sediment at high water in a macrotidal estuary*. J. Geophysical Res. 94: 14,395-14,405.

Uncles, R.J., M.L. Barton & J.A. Stephens 1996. *Seasonal variability of mobile mud deposits in the Tamar estuary*. In C. Pattiarachi (ed.), Mixing in Estuaries and Coastal Seas, Coastal and Estuarine Studies: 374-387. Washington, D.C.: American Geophysical Union.

Zimmerman, J.T.F. 1986. *The tidal whirlpool: a review of horizontal dispersion by tidal and residual currents*. Netherlands J. Sea Res. 20: 133-154.